

Monte Carlo methods and applications for the nuclear shell model

D.J. Dean* and J.A. White†

**Physics Division, Oak Ridge National Laboratory, Oak Ridge, TN
and Physics Department, University of Tennessee, Knoxville, TN*

†*W. K. Kellogg Radiation Laboratory, 106-38, California Institute of Technology
Pasadena, California 91125 USA*

Abstract. The shell-model Monte Carlo (SMMC) technique transforms the traditional nuclear shell-model problem into a path-integral over auxiliary fields. We describe below the method and its applications to four physics issues: calculations of *sd-pf*-shell nuclei, a discussion of electron-capture rates in *pf*-shell nuclei, exploration of pairing correlations in unstable nuclei, and level densities in rare earth systems.

I INTRODUCTION

Studies of nuclei far from stability have long been a goal of nuclear science. Nuclei on either side of the stability region, either neutron-rich or deficient, are being produced at new radioactive beam facilities across the world. At these facilities, and with the help of advances in nuclear many-body theory, the community will address many of the key physics issues including: mapping of the neutron and proton drip lines, thus exploring the limits of stability; understanding effects of the continuum on weakly bound nuclear systems; understanding the nature of shell gap modifications in very neutron-rich systems; determining nuclear properties needed for astrophysics; investigating deformation, spin, and pairing properties of systems far from stability; and analyzing microscopically unusual shapes in unstable nuclei.

The range and diversity of nuclear behavior, as indicated in the above list of ongoing and planned experimental investigations, have naturally engendered a host of theoretical models. Short of a complete solution to the many-nucleon problem, the interacting shell model is widely regarded as the most broadly capable description of low-energy nuclear structure, and the one most directly traceable to the fundamental many-body problem. Difficult though it may be, solving the shell-model problem is of fundamental importance to our understanding of the correlations found in nuclei.

One avenue of research during the past few years has been in the area of the nuclear shell model solved not by diagonalization, but by integration. In what follows,

we will describe the shell-model Monte Carlo (SMMC) method and discuss several recent and interesting results obtained from theory. These include calculations in *sd-pf*-shell neutron-rich nuclei, a discussion of electron-capture rates in *fp*-shell nuclei, pairing correlations in medium-mass nuclei near $N=Z$, and studies of level densities in rare-earth nuclei.

II SMMC METHODS

In the following we briefly outline the formalism of the SMMC method. We begin with a brief description of statistical mechanics techniques used in our approach, then discuss the Hubbard-Stratonovich transformation, and end with a discussion of Monte Carlo sampling procedures. We refer the reader to previous works [1,3] for a more detailed exposition.

A Observables

SMMC methods rely on an ability to calculate the imaginary-time many-body evolution operator, $\exp(-\beta H)$, where β is a real *c*-number. The many-body Hamiltonian can be written schematically as

$$H = \varepsilon \mathcal{O} + \frac{1}{2} V \mathcal{O} \mathcal{O}, \quad (1)$$

where \mathcal{O} is a density operator, V is the strength of the two-body interaction, and ε is a single-particle energy. In the full problem, there are many such quantities with various orbital indices that are summed over, but we omit them here for the sake of clarity.

While the SMMC technique does not result in a complete solution to the many-body problem in the sense of giving all eigenvalues and eigenstates of H , it can result in much useful information. For example, the expectation value of some observable, Ω , can be obtained by calculating

$$\langle \Omega \rangle = \frac{\text{Tr } e^{-\beta H} \Omega}{\text{Tr } e^{-\beta H}}. \quad (2)$$

Here, $\beta \equiv T^{-1}$ is interpreted as the inverse of the temperature T , and the many-body trace is defined as

$$\text{Tr } X \equiv \sum_i \langle i | X | i \rangle, \quad (3)$$

where the sum is over many-body states of the system. In the canonical ensemble, this sum is over all states with a specified number of nucleons (implemented by number projection [2,3]), while the grand canonical ensemble introduces a chemical potential and sums over *all* many-body states.

In the limit of low temperature ($T \rightarrow 0$ or $\beta \rightarrow \infty$), the canonical trace reduces to a ground-state expectation value. Alternatively, if $|\Phi\rangle$ is a many-body trial state not orthogonal to the exact ground state, $|\Psi\rangle$, then $e^{-\beta H}$ can be used as a filter to refine $|\Phi\rangle$ to $|\Psi\rangle$ as β becomes large. An observable can be calculated in this “zero temperature” method as

$$\frac{\langle \Phi | e^{-\frac{\beta}{2} H} \Omega e^{-\frac{\beta}{2} H} | \Phi \rangle}{\langle \Phi | e^{-\beta H} | \Phi \rangle} \xrightarrow{\beta \rightarrow \infty} \frac{\langle \Psi | \Omega | \Psi \rangle}{\langle \Psi | \Psi \rangle}. \quad (4)$$

If Ω is the Hamiltonian, then (4) at $\beta = 0$ is the variational estimate of the energy, and improves as β increases. Of course, the efficiency of the refinement for any observable depends upon the degree to which $|\Phi\rangle$ approximates $|\Psi\rangle$.

Beyond such static properties, $e^{-\beta H}$ allows us to obtain some information about the dynamical response of the system. For an operator Ω , the response function, $R_\Omega(\tau)$, in the canonical ensemble is defined as

$$R_\Omega(\tau) \equiv \frac{\text{Tr} e^{-(\beta-\tau)H} \Omega^\dagger e^{-\tau H} \Omega}{\text{Tr} e^{-\beta H}} \equiv \langle \Omega^\dagger(\tau) \Omega(0) \rangle, \quad (5)$$

where $\Omega^\dagger(\tau) \equiv e^{\tau H} \Omega^\dagger e^{-\tau H}$ is the imaginary-time Heisenberg operator. Interesting choices for Ω are the annihilation operators for particular orbitals, the Gamow-Teller, $M1$, or quadrupole moment, etc. Inserting complete sets of A -body eigenstates of H ($\{|i\rangle, |f\rangle\}$) with energies $E_{i,f}$ shows that

$$R_\Omega(\tau) = \frac{1}{Z} \sum_{if} e^{-\beta E_i} |\langle f | \Omega | i \rangle|^2 e^{-\tau(E_f - E_i)}, \quad (6)$$

where $Z = \sum_i e^{-\beta E_i}$ is the partition function. Thus, $R_\Omega(\tau)$ is the Laplace transform of the strength function $S_\Omega(E)$:

$$R_\Omega(\tau) = \int_{-\infty}^{\infty} e^{-\tau E} S_\Omega(E) dE; \quad (7)$$

$$S_\Omega(E) = \frac{1}{Z} \sum_{fi} e^{-\beta E_i} |\langle f | \Omega | i \rangle|^2 \delta(E - E_f + E_i). \quad (8)$$

Hence, if we can calculate $R_\Omega(\tau)$, $S_\Omega(E)$ can be determined. Short of a full inversion of the Laplace transform (which is often numerically difficult), the behavior of $R_\Omega(\tau)$ for small τ gives information about the energy-weighted moments of S_Ω . In particular,

$$R_\Omega(0) = \int_{-\infty}^{\infty} S_\Omega(E) dE = \frac{1}{Z} \sum_i e^{-\beta E_i} |\langle f | \Omega | i \rangle|^2 = \langle \Omega^\dagger \Omega \rangle_A \quad (9)$$

is the total strength,

$$-R'_{\Omega}(0) = \int_{-\infty}^{\infty} S_{\Omega}(E) E dE = \frac{1}{Z} \sum_{if} e^{-\beta E_i} |\langle f | \Omega | i \rangle|^2 (E_f - E_i) \quad (10)$$

is the first moment (the prime denotes differentiation with respect to τ).

It is important to note that we usually cannot obtain detailed spectroscopic information from SMMC calculations. Rather, we can calculate expectation values of operators in the thermodynamic ensembles or the ground state. Occasionally, these can indirectly furnish properties of excited states. For example, if there is a collective 2^+ state absorbing most of the $E2$ strength, then the centroid of the quadrupole response function will be a good estimate of its energy. But, in general, we are without the numerous specific excitation energies and wave functions that characterize a direct diagonalization. This is both a blessing and a curse. The former is that for the very large model spaces of interest, there is no way in which we can deal explicitly with all of the wave functions and excitation energies. Indeed, we often don't need to, as experiments only measure average nuclear properties at a given excitation energy. The curse is that comparison with detailed properties of specific levels is difficult. In this sense, the SMMC method is complementary to direct diagonalization for modest model spaces, but is the only method for treating very large problems.

B The Hubbard-Stratonovich transformation

It remains to describe the Hubbard-Stratonovich “trick” by which $e^{-\beta H}$ is managed. In broad terms, the difficult many-body evolution is replaced by a superposition of an infinity of tractable one-body evolutions, each in a different external field, σ . Integration over the external fields then reduces the many-body problem to quadrature.

To illustrate the approach, let us assume that only one operator \mathcal{O} appears in the Hamiltonian (1). Then all of the difficulty arises from the two-body interaction, that term in H quadratic in \mathcal{O} . If H were solely linear in \mathcal{O} , we would have a one-body quantum system, which is readily dealt with. To linearize the evolution, we employ the Gaussian identity

$$e^{-\beta H} = \sqrt{\frac{\beta |V|}{2\pi}} \int_{-\infty}^{\infty} d\sigma e^{-\frac{1}{2}\beta |V| \sigma^2} e^{-\beta h}; \quad h = \varepsilon \mathcal{O} + sV\sigma \mathcal{O}. \quad (11)$$

Here, h is a one-body operator associated with a c -number field σ , and the many-body evolution is obtained by integrating the one-body evolution, $U_{\sigma} \equiv e^{-\beta h}$, over all σ with a Gaussian weight. The phase, s , is 1 if $V < 0$, or i if $V > 0$. Equation (11) is easily verified by completing the square in the exponent of the integrand; since we have assumed that there is only a single operator \mathcal{O} , there is no need to worry about non-commutation.

For a realistic Hamiltonian, there will be many non-commuting density operators, \mathcal{O}_{α} , present, but we can always reduce the two-body term to diagonal form. Thus

for a general two-body interaction in a general time-reversal invariant form, we write

$$H = \sum_{\alpha} (\epsilon_{\alpha}^* \bar{\mathcal{O}}_{\alpha} + \epsilon_{\alpha} \mathcal{O}_{\alpha}) + \frac{1}{2} \sum_{\alpha} V_{\alpha} \{ \mathcal{O}_{\alpha}, \bar{\mathcal{O}}_{\alpha} \}, \quad (12)$$

where $\bar{\mathcal{O}}_{\alpha}$ is the time reverse of \mathcal{O}_{α} . Since, in general, $[\mathcal{O}_{\alpha}, \mathcal{O}_{\beta}] \neq 0$, we must split the interval β into N_t “time slices” of length $\Delta\beta \equiv \beta/N_t$,

$$e^{-\beta H} = [e^{-\Delta\beta H}]^{N_t}, \quad (13)$$

and for each time slice $n = 1, \dots, N_t$ perform a linearization similar to Eq. 11 using auxiliary fields $\sigma_{\alpha n}$. Note that because the various \mathcal{O}_{α} need not commute, the representation of $e^{-\Delta\beta h}$ must be accurate through order $(\Delta\beta)^2$ to achieve an overall accuracy of order $\Delta\beta$.

We are now able to write expressions for observables as the ratio of two field integrals. Thus expectations of observables can be written as

$$\langle \Omega \rangle = \frac{\int \mathcal{D}\sigma W_{\sigma} \Omega_{\sigma}}{\int \mathcal{D}\sigma W_{\sigma}}, \quad (14)$$

where

$$\begin{aligned} W_{\sigma} &= G_{\sigma} \text{Tr} U_{\sigma}; & G_{\sigma} &= e^{-\Delta\beta \sum_{\alpha n} |V_{\alpha}| |\sigma_{\alpha n}|^2}; \\ \Omega_{\sigma} &= \frac{\text{Tr} U_{\sigma} \Omega}{\text{Tr} U_{\sigma}}; & \mathcal{D}\sigma &\equiv \prod_{n=1}^{N_t} \prod_{\alpha} d\sigma_{\alpha n} d\sigma_{\alpha n}^* \left(\frac{\Delta\beta |V_{\alpha}|}{2\pi} \right), \end{aligned} \quad (15)$$

and

$$\begin{aligned} U_{\sigma} &= U_{N_t} \dots U_2 U_1; & U_n &= e^{-\Delta\beta h_n}; \\ h_n &= \sum_{\alpha} (\epsilon_{\alpha}^* + s_{\alpha} V_{\alpha} \sigma_{\alpha n}) \bar{\mathcal{O}}_{\alpha} + (\epsilon_{\alpha} + s_{\alpha} V_{\alpha} \sigma_{\alpha n}^*) \mathcal{O}_{\alpha}. \end{aligned} \quad (16)$$

This is, of course, a discrete version of a path integral over σ . Because there is a field variable for each operator at each time slice, the dimension of the integrals $\mathcal{D}\sigma$ can be very large, often exceeding 10^5 . The errors in Eq. 14 are of order $\Delta\beta$, so that high accuracy requires large N_t and perhaps extrapolation to $N_t = \infty$ ($\Delta\beta = 0$).

Thus, the many-body observable is the weighted average (weight W_{σ}) of the observable Ω_{σ} calculated in an ensemble involving only the one-body evolution U_{σ} . Similar expressions involving two σ fields (one each for $e^{-\tau H}$ and $e^{-(\beta-\tau)H}$) can be written down for the response function (5), and all are readily adapted to the canonical or grand canonical ensembles or to the zero-temperature case.

An expression of the form (14) has a number of attractive features. First, the problem has been reduced to quadrature—we need only calculate the ratio of two integrals. Second, all of the quantum mechanics (which appears in Ω_{σ}) is of the one-body variety, which is simply handled by the algebra of $N_s \times N_s$ matrices. The price to pay is that we must treat the one-body problem for all possible σ fields.

C Monte Carlo quadrature and the sign problem

We employ the Metropolis, Rosenbluth, Rosenbluth, Teller, and Teller algorithm [4] to generate the field configurations, σ , which requires only the ability to calculate the weight function for a given value of the integration variables. This method requires that the weight function W_σ must be real and non-negative. Unfortunately, many of the Hamiltonians of physical interest suffer from a sign problem, in that W_σ is negative over significant fractions of the integration volume. The fractional variance of a given expectation value becomes unacceptably large as the average sign approaches zero.

It was shown [3] that for even-even and $N = Z$ nuclei there is no sign problem for Hamiltonians if all $V_\alpha \leq 0$. Such forces include reasonable approximations to the realistic Hamiltonian like pairing-plus-multipole interactions. However, for an arbitrary Hamiltonian, we are not guaranteed that all $V_\alpha \leq 0$ (see, for example, Alhassid *et al.* [6]). However, we may expect that a *realistic* Hamiltonian will be dominated by terms like those of the schematic pairing-plus-multipole force (which is, after all, why the schematic forces were developed) so that it is, in some sense, close to a Hamiltonian for which the MC is directly applicable. Thus, the “practical solution” to the sign problem presented in Alhassid *et al.* [6] is based on an extrapolation of observables calculated for a “nearby” family of Hamiltonians whose integrands have a positive sign. Success depends crucially upon the degree of extrapolation required. Empirically, one finds that for all of the many realistic interactions tested in the *sd*- and *pf*-shells, the extrapolation required is modest, amounting to a factor-of-two variation in the isovector monopole pairing strength.

Based on the above observation, it is possible to decompose H in Eq. 12 into its “good” and “bad” parts, $H = H_G + H_B$. The “good” Hamiltonian, H_G , includes, in addition to the one-body terms, all the two-body interactions with $V_\alpha \leq 0$, while the “bad” Hamiltonian, H_B , contains all interactions with $V_\alpha > 0$. By construction, calculations with H_G alone have $\Phi_\sigma \equiv 1$ and are thus free of the sign problem.

We define a family of Hamiltonians, H_g , that depend on a continuous real parameter g as $H_g = f(g)H_G + gH_B$, so that $H_{g=1} = H$, and $f(g)$ is a function with $f(1) = 1$ and $f(g < 0) > 0$ that can be chosen to make the extrapolations less severe. (In practical applications, $f(g) = 1 - (1 - g)/\chi$ with $\chi \approx 4$, and applied only to the two-body terms in H_G has been found to be a good choice.) If the V_α that are large in magnitude are “good,” we expect that $H_{g=0} = H_G$ is a reasonable starting point for the calculation of an observable $\langle \Omega \rangle$. One might then hope to calculate $\langle \Omega \rangle_g = \text{Tr}(\Omega e^{-\beta H_g}) / \text{Tr}(e^{-\beta H_g})$ for small $g > 0$ and then to extrapolate to $g = 1$, but typically $\langle \Phi \rangle$ collapses even for small positive g . However, it is evident from our construction that H_g is characterized by $\Phi_\sigma \equiv 1$ for any $g \leq 0$, since all the “bad” $V_\alpha (> 0)$ are replaced by “good” $gV_\alpha < 0$. We can therefore calculate $\langle \Omega \rangle_g$ for any $g \leq 0$ by a Monte Carlo sampling that is free of the sign problem. If $\langle \Omega \rangle_g$ is a smooth function of g , it should then be possible to extrapolate to $g = 1$ (i.e., to the original Hamiltonian) from $g \leq 0$. We emphasize that $g = 0$ is not expected to be a singular point of $\langle \Omega \rangle_g$; it is special only in the Monte Carlo eval-

uation. The extrapolation methods we employ have been tested against standard shell-model diagonalizations in many cases, and have, in general, been shown to work very well [3].

III APPLICATIONS

A *sd-pf* nuclei

Studies of extremely neutron-rich nuclei have revealed a number of intriguing new phenomena. Two sets of these nuclei that have received particular attention are those with neutron number N in the vicinity of the $1s0d$ and $0f_{7/2}$ shell closures ($N \approx 20$ and $N \approx 28$). Experimental studies of neutron-rich Mg and Na isotopes indicate the onset of deformation, as well as the modification of the $N = 20$ shell gap for ^{32}Mg and nearby nuclei [7]. Inspired by the rich set of phenomena occurring near the $N = 20$ shell closure when $N \gg Z$, attention has been directed to nuclei near the $N = 28$ (sub)shell closure for a number of S and Ar isotopes [8,9] where similar, but less dramatic, effects have been seen as well.

In parallel with the experimental efforts, there have been several theoretical studies seeking to understand and, in some cases, predict properties of these unstable nuclei. Both mean-field [10,11] and shell-model calculations [8,9,12–16] have been proposed. The latter require a severe truncation to achieve tractable model spaces, since the successful description of these nuclei involves active nucleons in both the *sd*- and the *pf*-shells. The natural basis for the problem is therefore the full *sd-pf* space, which puts it out of reach of exact diagonalization on current hardware.

SMMC methods offer an alternative to direct diagonalization when the bases become very large. Though SMMC provides limited detailed spectroscopic information, it can predict, with good accuracy, overall nuclear properties such as masses, total strengths, strength distributions, and deformation — precisely those quantities probed by the recent experiments. It thus seems natural to apply SMMC methods to these unstable neutron-rich nuclei. Two questions will arise — center-of-mass motion and choice of the interaction — that are not exactly new, but demand special treatment in very large spaces. These questions were addressed in detail in Ref. [17]. We present a brief selection of results here.

There is limited experimental information about the highly unstable, neutron-rich nuclei under consideration. In many cases only the mass, excitation energy of the first excited state, the $B(E2)$ to that state, and the β -decay rate is known, and not even all of this information is available in some cases. From the measured $B(E2)$, an estimate of the nuclear deformation parameter, β_2 , has been obtained via the usual relation

$$\beta_2 = 4\pi \sqrt{B(E2; 0_{gs}^+ \rightarrow 2_1^+)}/3ZR_0^2e \quad (17)$$

with $R_0 = 1.2A^{1/3}$ fm and $B(E2)$ given in $e^2\text{fm}^4$.

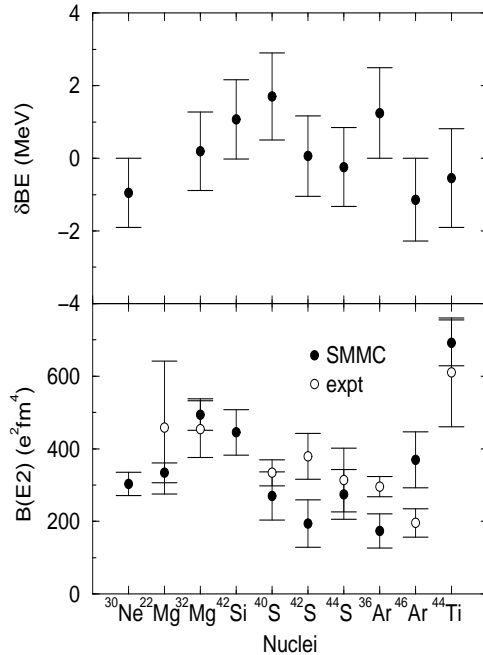


FIGURE 1. Top: Difference between theoretical and experimental binding energies for the *sd-pf*-shell nuclei studied in this work. Bottom: Experimental and theoretical $B(E2)$ values.

Much of the interest in the region stems from the unexpectedly large values of the deduced β_2 , results which suggest the onset of deformation and have led to speculations about the vanishing of the $N = 20$ and $N = 28$ shell gaps. The lowering in energy of the 2_1^+ state supports this interpretation. The most thoroughly studied case, and the one which most convincingly demonstrates these phenomena, is ^{32}Mg with its extremely large $B(E2) = 454 \pm 78 e^2\text{fm}^4$ and corresponding $\beta_2 = 0.513$ [7]; however, a word of caution is necessary when deciding on the basis of this limited information that we are in the presence of well-deformed rotors: for ^{22}Mg , we would obtain $\beta_2 = 0.67$, even more spectacular, and for ^{12}C , $\beta_2 = 0.8$, well above the superdeformed bands.

Most of the measured observables can be calculated within the SMMC framework. It is well known that in *deformed* nuclei the total $B(E2)$ strength is almost saturated by the $0_{gs}^+ \rightarrow 2_1^+$ transition (typically 80% to 90% of the strength lies in this transition). Thus the total strength calculated by SMMC should only slightly overestimate the strength of the measured transition. In Fig. 1 the SMMC computed $B(E2, total)$ values are compared to the experimental $B(E2; 0_{gs}^+ \rightarrow 2_1^+)$ values. Reasonable agreement with experimental data across the space is obtained when one chooses effective charges of $e_p = 1.5$ and $e_n = 0.5$. Using these same effective charges, the USD values for the $B(E2, 0_{gs}^+ \rightarrow 2_1^+)$ of the *sd*-shell nuclei ^{32}Mg and ^{30}Ne are 177.1 and 143.2 $e^2\text{fm}^4$, respectively, far lower than the full *sd-pf* calculated and experimental values. All of the theoretical calculations require excitations to the *pf*-shell before reasonable values can be obtained. We note a

TABLE 1. Comparisons of the SMMC electron capture rates with the total (λ_{ec}) and partial Gamow-Teller (λ_{ec}^{GT}) rates as given in Ref. [19]. Physical conditions at which the comparisons were made are $\rho_7 = 5.86$, $T_9 = 3.40$, and $Y_e = 0.47$ for the upper part of the table, and $\rho_7 = 10.7$, $T_9 = 3.65$, and $Y_e = 0.455$ for the lower part.

Nucleus	λ_{ec} (sec ⁻¹) (SMMC)	λ_{ec} (sec ⁻¹) (Ref. [19])	λ_{ec}^{GT} (sec ⁻¹) (Ref. [19])
⁵⁵ Co	3.89E-04	1.41E-01	1.23E-01
⁵⁷ Co	3.34E-06	3.50E-03	1.31E-04
⁵⁵ Fe	1.20E-08	1.61E-03	1.16E-07
⁵⁶ Ni	3.47E-02	1.60E-02	6.34E-03
⁵⁸ Ni	1.01E-03	6.36E-04	4.04E-06
⁶⁰ Ni	7.39E-05	1.49E-06	4.86E-07
⁵⁹ Co	3.44E-07	2.09E-04	6.37E-05
⁵⁷ Co	2.06E-05	7.65E-03	3.69E-04
⁵⁵ Fe	1.07E-07	3.80E-03	5.51E-07
⁵⁶ Fe	9.80E-06	4.68E-07	6.60E-10
⁵⁴ Fe	3.84E-04	9.50E-04	3.85E-06
⁵¹ V	1.06E-06	1.24E-05	9.46E-09
⁵² Cr	1.32E-04	2.01E-07	1.59E-10
⁶⁰ Ni	3.61E-04	7.64E-06	2.12E-06

general agreement among all calculations of the $B(E2)$ for ⁴⁶Ar, although they are typically larger than experimental data would suggest. We also note a somewhat lower value of the $B(E2)$ in this calculation as compared to experiment and other theoretical calculations in the case of ⁴²S [15].

Also shown in Fig. 1 are the differences between experimental and theoretical binding energies for nuclei in this region. Agreement is quite good overall. Further details of the interaction and results may be found in [17].

B Electron capture rates for Fe-region nuclei

The impact of nuclear structure on astrophysics has become increasingly important, particularly in the fascinating, and presently unsolved, problem of type-II supernovae explosions. One key ingredient of the precollapse scenario is the electron-capture cross section on nuclei [18,19]. An important contribution to electron-capture cross sections in supernovae environments is the Gamow-Teller (GT) strength distribution. This strength distribution, calculated in SMMC using Eqs. (3 and 4) above, is used to find the energy-dependent cross section for electron capture. In order to obtain the electron-capture rates, the cross section is then folded with the flux of a degenerate relativistic electron gas [20]. Note that the

Gamow-Teller distribution is calculated at the finite nuclear temperature which, in principle, is the same as the one for the electron gas.

It is important to calculate the GT strength distributions reasonably accurately for both the total strength and the position of the main GT peak in order to have a quantitative estimate for the electron-capture rates. For astrophysical purposes, calculating the rates to within a factor of two is required. We concentrate here on mid- fp -shell results for the electron-capture cross sections [20]. The Kuo-Brown interaction [21], modified in the monopole terms by Zuker and Poves [22], was used throughout these pf -shell calculations. This interaction reproduces quite nicely the ground- and excited-state properties of mid- fp -shell nuclei [23,24], including the total Gamow-Teller strengths and distributions, where the overall agreement between theory and experiment [25] is quite reasonable. The SMMC technique allows one to probe the complete $0\hbar\omega$ fp -shell region without any parameter adjustments to the Hamiltonian, although the Gamow-Teller operator has been renormalized by the standard factor of 0.8.

Do the electron-capture rates presented here indicate potential implications for the precollapse evolution of a type II supernova? To make a judgment on this important question, one should compare in Table I the SMMC rates for selected nuclei with those currently used in collapse calculations [19]. For the comparison, we choose the same physical conditions as assumed in Tables 4–6 in Aufderheide *et al.* [19]. Table I also lists the partial electron-capture rate which has been attributed to Gamow-Teller transitions [19]. Note that for even-parent nuclei, the present rate approximately agrees with the currently recommended *total* rate. A closer inspection, however, shows significant differences between the present rate and the one attributed to the Gamow-Teller transition in Aufderheide *et al.* [19]. The origin of this discrepancy is due to the fact that Fuller *et al.* [26] places the Gamow-Teller resonance for even-even nuclei systematically at too high an excitation energy. This shortcoming has been corrected in Fuller *et al.* [26] and Aufderheide *et al.* [19] by adding an experimentally known low-lying strength in addition to the one attributed to Gamow-Teller transitions. However, the overall good agreement between the SMMC results for even-even nuclei and the recommended rates indicates that the SMMC approach also accounts correctly for this low-lying strength. This has already been deduced from the good agreement between SMMC Gamow-Teller distributions and data including the low-energy regime [25].

Thus, for even-even nuclei, the SMMC approach is able to predict the *total* electron-capture rate rather reliably, even if no experimental data are available. Note that the SMMC rate is somewhat larger than the recommended rate for ^{56}Fe and ^{60}Ni . In both cases, the experimental Gamow-Teller distribution is known and agrees well with the SMMC results [25]. While the proposed increase of the rate for ^{60}Ni is not expected to have noticeable influence on the pre-collapse evolution, the increased rate for ^{56}Fe makes this nucleus an important contributor in the change of Y_e during the collapse (see Table 15 of Aufderheide *et al.* [19]).

For electron capture on odd- A nuclei, observe that the SMMC rates, derived from the Gamow-Teller distributions, are significantly smaller than the recommended to-

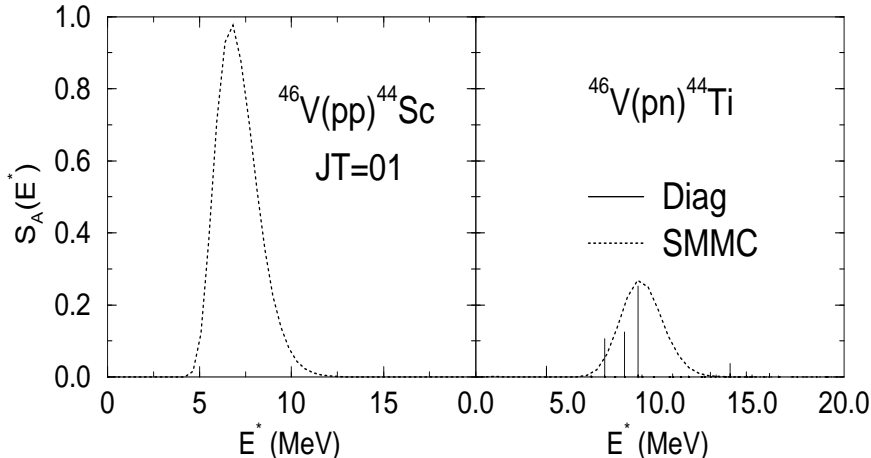


FIGURE 2. Left: proton pair strength distribution for ^{46}V . Right: proton-neutron ($T=1$) pair strength distribution. SMMC: thick line; direct diagonalization: impulses.

tal rate. This is due to the fact that for odd- A nuclei the Gamow-Teller transition peaks at rather high excitation energies in the daughter nucleus. The electron-capture rate on odd- A nuclei is therefore carried by weak transitions at low excitation energies. Comparing the SMMC rates to those attributed to Gamow-Teller transitions in Fuller *et al.* [26] and Aufderheide *et al.* [19] reveals that the latter have been, in general, significantly overestimated, which is caused by the fact that the position of the Gamow-Teller resonance is usually put at too low excitation energies in the daughter. The SMMC calculation implies that the Gamow-Teller transitions should not contribute noticeably to the electron-capture rates on odd- A nuclei at the low temperatures studied in Tables 14–16 in Aufderheide *et al.* [19]. Thus, the rates for odd- A nuclei given in these tables should generally be replaced by the non-Gamow-Teller fraction.

C Pair correlations in nuclei

We would now like to turn to the subject of pair correlations in nuclei, and calculations aimed at their understanding. Nuclei near $N=Z$ offer a unique place to study proton-neutron pairing, particularly in the isospin $T=1$ channel. In fact, most heavy odd-odd, $N=Z$ nuclei beyond ^{40}Ca have total spin $J=0$, $T=1$ ground states. Theoretical studies have shown that many of these nuclei have enhanced $T=1$ proton-neutron correlations when compared to their even-even counterparts. These correlations are, to a lesser extent, present in even-even systems, but tend to decrease as one moves away from $N=Z$. In at least one nucleus in the mass 70 region, ^{74}Rb , there is experimental evidence for a ground state $T=1$ band [27].

Experimentally, pair correlations can best be measured by pair transfer on nuclei. Although total cross sections are typically underpredicted when one employs spectroscopic factors computed from the shell model, relative two-nucleon spectro-

spectroscopic factors within one nucleus are more reliable. Therefore, it is necessary for one to calculate and measure pair transfer from both the ground and excited states in a nucleus.

The SMMC method may be used to calculate the strength distribution of the pair annihilation operator A_{JT_z} , as defined in Koonin *et al.* [3]. The total strength of these pairing operators, i.e. the expectation $\langle A_{JT}^\dagger A_{JT} \rangle$, has been studied previously as a function of mass, temperature [28,29], and rotation [30]. We would like to briefly present here the strength distributions of the pair operators as calculated in SMMC. The strength distribution for the pair transfer spectroscopic factors is proportional to $\langle A - 2 | A_{JT} | A \rangle$ and is calculated by the inversion of Eq. (4).

In future work, we will discuss the strength distributions in detail. Here we would like to briefly conclude by demonstrating that the SMMC results and the direct diagonalization results agree very nicely for the proton pair strength distributions in the ground state of ^{46}V . This is demonstrated in the left panel of Fig. 2. Shown in the right panel is the isovector proton-neutron pairing strength distribution with respect to the daughter nucleus. Notice that the overall strength is much larger in the proton-neutron channel, as discussed previously in Langanke *et al.* [29], and that the peak is several MeV lower in excitation relative to the like-particle channel. In both cases the strength distribution in ^{46}V differs significantly from that found in ^{48}Cr , where one finds that the dominant component is a ground-state to ground-state transition involving mainly particles in the $0f_{7/2}$ single-particle state. In both odd-odd $N=Z$ channels, the distribution is fairly highly fragmented.

D Rare earth nuclei

We have recently applied SMMC techniques to survey rare-earth nuclei in the Dy region. This extensive study formed the thesis topic of J.A. White [36], whose goal was to examine how the phenomenologically motivated “pairing-plus-quadrupole” interaction compares in exact shell-model solutions with other methods. We also examined how the shell-model solutions compare with experimental data; static path approximation (SPA) calculations were also performed. There have been efforts recently by others to use SPA calculations, since they are simpler and faster (see [37,38] as examples). However, we found that SPA results are not consistently good. This study was also designed to investigate whether the phenomenological pairing-plus-quadrupole-type interactions can be used in exact solutions for large model spaces, and whether the interaction parameters require significant renormalization when using SPA.

We discuss here one particular aspect of that work, namely level density calculations. Details may be found in [39]. We used the Kumar-Baranger Hamiltonian with parameters appropriate for this region. Our single-particle space included the 50-82 subshell for the protons and the 82-126 shell for the neutrons. While several interesting aspects of these systems were studied in SMMC, we limit our discussion here to the level densities obtained for ^{162}Dy .

SMMC is an excellent way to calculate level densities. $E(\beta)$ is calculated for many values of β which determine the partition function, Z , as

$$\ln[Z(\beta)/Z(0)] = - \int_0^\beta d\beta' E(\beta') \quad (18)$$

$Z(0)$ is the total number of available states in the space. The level density is then computed as an inverse Laplace transform of Z . Here, the last step is performed with a saddle point approximation with $\beta^{-2}C \equiv -dE/d\beta$:

$$S(E) = \beta E + \ln Z(\beta) \quad (19)$$

$$\rho(E) = (2\pi\beta^{-2}C)^{-1/2} \exp(S) \quad (20)$$

SMMC has been used recently to calculate level density in iron region nuclei [40], and here we demonstrate its use in the rare-earth region.

The comparison of SMMC density in ^{162}Dy with the Tveter et al. [41] data is displayed in Fig. 3. The experimental method can reveal fine structure, but does not determine the absolute density magnitude. The SMMC calculation is scaled by a factor to facilitate comparison. In this case, the factor has been chosen to make the curves agree at lower excitation energies. From 1-3 MeV, the agreement is very good. From 3-5 MeV, the SMMC density increases more rapidly than the data. This deviation from the data cannot be accounted for by statistical errors in either the calculation or measurement. Near 6 MeV, the measured density briefly flattens before increasing and this also appears in the calculation, but the measurement errors are larger at that point.

The measured density includes all states included in the theoretical calculation plus some others, so that one would expect the measured density to be greater than or equal to the calculated density and never smaller. We may have instead chosen our constant to match the densities for moderate excitations and let the measured density be higher than the SMMC density for lower energies (1-3 MeV). Comparing structure between SMMC and data is difficult for the lowest energies due to statistical errors in the calculation and comparison at the upper range of the SMMC calculation, i.e., $E \approx 15$ MeV, is unfortunately impossible since the data only extend to about 8 MeV excitation energy.

IV CONCLUSIONS

In these Proceedings, we have used four specific examples (there are several others) for which the SMMC calculations have proven very useful in understanding the properties of nuclei in systems where the number of valence particles prohibits the use of more traditional approaches. The method has proven to be a valuable tool for furthering our understanding of nuclear structure and astrophysics. Continued developments in both creating useful interactions and shell-model technology should continue to enhance our ability to understand nuclei far from stability in the coming years.

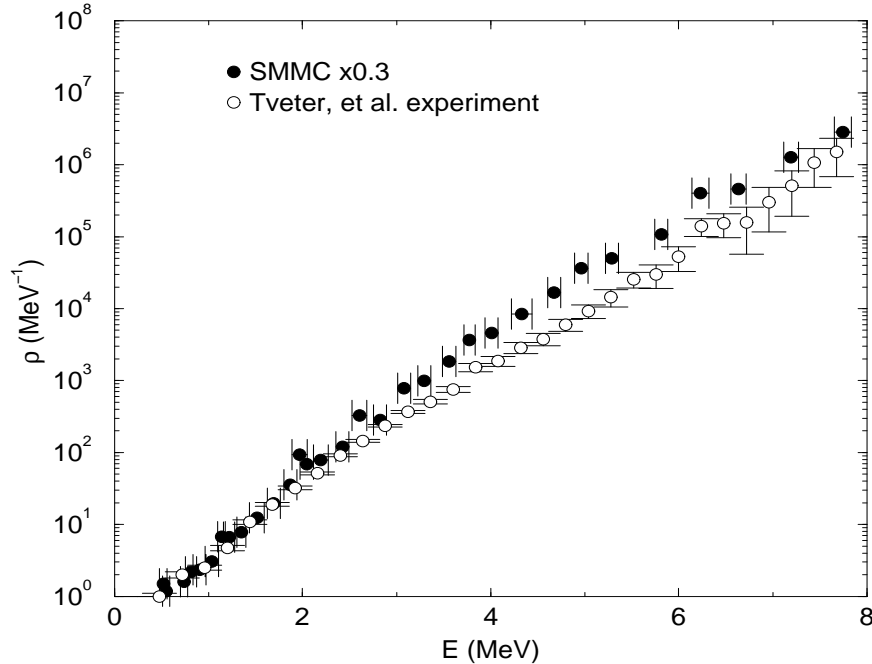


FIGURE 3. SMMC density vs. experimental data in ^{162}Dy .

ACKNOWLEDGMENTS

Oak Ridge National Laboratory (ORNL) is managed by Lockheed Martin Energy Research Corp. for the U.S. Department of Energy under contract number DE-AC05-96OR22464. This work was supported in part through grant DE-FG02-96ER40963 from the U.S. Department of Energy. This work was supported in part by the National Science Foundation, Grants No. PHY-9722428, PHY-9420470, and PHY-9412818.

REFERENCES

1. G. H. Lang, C. W. Johnson, S. E. Koonin, and W. E. Ormand, *Phys. Rev.* **C48**, 1518 (1993).
2. W. E. Ormand, D. J. Dean, C. W. Johnson, G. H. Lang, and S. E. Koonin, *Phys. Rev.* **C49**, 1422 (1994).
3. S. E. Koonin, D. J. Dean, and K. Langanke, *Phys. Repts.* **278**, 1 (1997), and references therein.
4. N. Metropolis, A. Rosenbluth, M. Rosenbluth, A. Teller, and E. Teller, *J. Chem. Phys.* **21**, 1087 (1953).
5. E. Y. Loh, Jr. and J. E. Gubernatis, in *Electronic Phase Transitions*, ed. W. Hanke and Yu.V. KopaeV, 177 (1992).
6. Y. Alhassid, D. J. Dean, S. E. Koonin, G. H. Lang, and W. E. Ormand, *Phys. Rev. Lett.* **72**, 613 (1994).

7. T. Motobayashi et al., *Phys. Lett.* **B346**, 9 (1995).
8. H. Scheit et al., *Phys. Rev. Lett.* **77**, 3967 (1996).
9. T. Glasmacher et al., *Phys. Lett.* **B395**, 163 (1997).
10. T. R. Werner et al., *Nucl. Phys.* **A597**, 327 (1996).
11. X. Campi, H. Flocard, A. K. Kerman, and S. E. Koonin, *Nucl. Phys.* **A251**, 193 (1975).
12. E. K. Warburton, J. A. Becker, and B. A. Brown, *Phys. Rev.* **C41**, 1147 (1990).
13. A. Poves and J. Retamosa, *Nucl. Phys.* **A571**, 221 (1994).
14. N. Fukunishi, T. Otsuka, and T. Sebe, *Phys. Lett.* **B296**, 279 (1992).
15. J. Retamosa, E. Caurier, F. Nowacki, and A. Poves, *Phys. Rev.* **C55**, 1266 (1997).
16. E. Caurier, F. Nowacki, A. Poves, and J. Retamosa, *Phys. Rev.* **C58**, 2033 (1998).
17. D. J. Dean, M. T. Ressel, M. Hjorth-Jensen, S. E. Koonin, K. Langanke, and A. Zuker, submitted to *Phys. Rev. C* (1998).
18. H. A. Bethe, *Rev. Mod. Phys.* **62**, 801 (1990).
19. M. B. Aufderheide, I. Fushiki, S. E. Woosley, and D. H. Hartman, *Astrophys. J. Supp.* **91**, 389 (1994).
20. D. J. Dean, K. Langanke, L. Chatterjee, P. B. Radha, and M. R. Strayer, *Phys. Rev.* **C58**, 536 (1998).
21. T.T.S. Kuo and G. E. Brown, *Nucl. Phys.* **A114**, 241 (1968).
22. A. Poves and A. Zuker, *Phys. Repts.* **70**, 235 (1981).
23. E. Caurier, A. Zuker, A. Poves, and G. Martinez-Pinedo, *Phys. Rev.* **C50**, 225 (1994).
24. K. Langanke, D. J. Dean, P. B. Radha, Y. Alhassid, and S. E. Koonin, *Phys. Rev.* **C52**, 718 (1995).
25. P. B. Radha, D. J. Dean, S. E. Koonin, K. Langanke, and P. Vogel, *Phys. Rev.* **C56**, 3079 (1997).
26. G. M. Fuller, W. A. Fowler, and M. J. Newman, *Astrophys. J.* **48**, 279 (1982).
27. D. Rudolph et al., *Phys. Rev. Lett.* **76**, 376 (1996).
28. K. Langanke, D. J. Dean, P. B. Radha, and S. E. Koonin, *Nucl. Phys.* **A602**, 244 (1996).
29. K. Langanke, D. J. Dean, P. B. Radha, and S. E. Koonin, *Nucl. Phys.* **A613**, 253 (1997).
30. D. J. Dean, S. E. Koonin, K. Langanke, and P. B. Radha, *Phys. Lett.* **B399**, 1 (1997)
31. L. Wilets and M. Jean, *Phys. Rev.* **102**, 788 (1956).
32. O. K. Vorov and V. G. Zelevinsky, *Nucl. Phys.* **A439**, 207 (1985).
33. W. Krips et al., *Nucl. Phys.* **A529**, 485 (1991).
34. T. Otsuka, *Nucl. Phys.* **A557**, 531c (1993).
35. Y. Alhassid, G. Bertsch, D. J. Dean, and S. E. Koonin, *Phys. Rev. Lett.* **77**, 1444 (1996).
36. J. A. White, Ph.D. Thesis, California Institute of Technology, 1998.
37. R. Rossignoli, *Phys. Rev.* **C54**, 3 (1996).
38. R. Rossignoli, N. Canosa, and J. L. Egido, *Nucl. Phys.* **A607**, 3 (1996).
39. J. A. White, S. E. Koonin, and D. J. Dean, submitted to *Phys. Rev. C* (1998).
40. H. Nakada and Y. Alhassid, *Phys. Rev. Lett.* **79**, 16 (1997).
41. T. Tveter et al., *Phys. Rev. Lett.* **77**, 2404 (1996).